



# Characterization of Cerebellar Atrophy and Resting State Functional Connectivity Patterns in Sporadic Adult-Onset Ataxia of Unknown Etiology (SAOA)

Xueyan Jiang<sup>1</sup> · J. Faber<sup>1,2</sup> · I. Giordano<sup>1,2</sup> · J. Machts<sup>3,4</sup> · Ch. Kindler<sup>1,2</sup> · A. Dudsek<sup>5</sup> · O. Speck<sup>3</sup> · Ch. Kamm<sup>5</sup> · E. Düzel<sup>3,4</sup> · F. Jessen<sup>1,6</sup> · A. Spottke<sup>1,2</sup> · St. Vielhaber<sup>3,4</sup> · H. Boecker<sup>1,7</sup> · T. Klockgether<sup>1,2</sup> · L. Scheef<sup>1,7</sup>

Published online: 17 August 2019

© Springer Science+Business Media, LLC, part of Springer Nature 2019

## Abstract

Sporadic adult-onset ataxia of unknown etiology (SAOA) is a non-genetic neurodegenerative disorder of the cerebellum of unknown cause which manifests with progressive ataxia without severe autonomic failure. Although SAOA is associated with cerebellar degeneration, little is known about the specific cerebellar atrophy pattern in SAOA. Thirty-seven SAOA patients and 49 healthy controls (HCs) were included at two centers. We investigated the structural and functional characteristics of SAOA brains using voxel-based morphometry (VBM) and resting-state functional imaging (rs-fMRI). In order to examine the functional consequence of structural cerebellar alterations, the amplitude of low-frequency fluctuation (ALFF) and degree centrality (DC) were analyzed, and then assessed their relation with disease severity, disease duration, and age of onset within these regions. Group differences were investigated using two-sample *t* tests, controlling for age, gender, site, and the total intracranial volume. The VBM analysis revealed a significant, mostly bilateral reduction of local gray matter (GM) volume in lobules I–V, V, VI, IX, X, and vermis VIII a/b in SAOA patients, compared with HCs. The GM volume loss in these regions was significantly associated with disease severity, disease duration, and age of onset. The disease-related atrophy regions did not show any functional alternations compared with HCs but were functionally characterized by high ALFF and poor DC compared with intact cerebellar regions. Our data revealed volume reduction in SAOA in cerebellar regions that are known to be involved in motor and somatosensory processing, corresponding with the clinical phenotype of SAOA. Our data suggest that the atrophy occurs in those cerebellar regions which are characterized by high ALFF and poor DC. Further studies have to show if these findings are specific for SAOA, and if they can be used to predict disease progression.

**Keywords** SAOA · Cerebellum · Structural MRI · Functional MRI

---

**Electronic supplementary material** The online version of this article (<https://doi.org/10.1007/s12311-019-01072-y>) contains supplementary material, which is available to authorized users.

---

✉ Xueyan Jiang  
Xueyan.Jiang@dzne.de

<sup>1</sup> Clinical Research, German Center for Neurodegenerative Diseases (DZNE), Bonn, Germany

<sup>2</sup> Department of Neurology, University Hospital Bonn, Bonn, Germany

<sup>3</sup> German Center for Neurodegenerative Diseases (DZNE), Magdeburg, Germany

<sup>4</sup> Department of Neurology, Otto-von-Guericke University, Magdeburg, Germany

<sup>5</sup> Department of Neurology, University of Rostock, Rostock, Germany

<sup>6</sup> Department of Psychiatry, Medical Faculty, University of Cologne, Cologne, Germany

<sup>7</sup> Department of Radiology, University of Bonn, Bonn, Germany

## Introduction

Sporadic adult-onset ataxia of unknown etiology (SAOA) is a non-genetic neurodegenerative disorder of the cerebellum of unknown cause [1–3]. Ataxia typically starts in the fifth decade with a steady, but comparably slow progression [2, 3]. Patients are characterized by predominant cerebellar ataxia including impaired gait and stance, poor coordination, and dysarthria. The cerebellar cortex degeneration hypothesis was confirmed by some autopsied cases that the degeneration results from prominent Purkinje neuron loss in the cerebellum [4]. Neuroimaging studies in SAOA observed a prominent volume loss in the cerebellum [1], but due to a lack of a high-resolution human cerebellar atlas template, a specific spatial pattern has not yet been established for SAOA. In particular, it remained unclear how cerebellar atrophy is related to clinical features, and how it affects the cerebellar functional connectivity in SAOA patients.

In order to examine structural and functional changes of the cerebellum in more detail, we acquired high-resolution T1-weighted MRI data sets as well as resting-state fMRI in a large cohort of SAOA patients and healthy controls (HCs) within a large multicenter study. Using a high-resolution cerebellar template, provided by SUIIT [5], we wanted to establish a more accurate disease-related atrophy pattern and to investigate how local atrophy impacts the intra-cerebellar functional connectivity. Amplitude of low-frequency fluctuation (ALFF), reflecting regional spontaneous synchronous neural activity [6, 7] and degree centrality (DC), a graph-based measure on how strong a certain region is connected to other regions [8, 9] were chosen due to their ability to detect functional changes in clinical applications [10].

The goal of this study was to characterize disease-related gray matter abnormalities in the cerebellum in SAOA patients and to determine the relationship of local cerebellar neurodegeneration with clinical variables and intra-cerebellar functional connectivity patterns.

## Materials and Methods

The study was approved by the local ethics committees in Bonn and Magdeburg. All subjects provided written informed consent before participation.

### Participants

This study is based on a multicenter natural history study on sporadic adult-onset degenerative ataxia (SPORTAX, [ClinicalTrials.gov](https://clinicaltrials.gov/ct2/show/study/NCT02701036) registration: NCT02701036). The inclusion criteria are defined as follows: (1) progressive ataxia; (2) disease onset after the age of 40 years; (3) informative and negative family history. Participants were excluded if (1)

ataxia could be explained by an established cause (e.g., chronic alcohol abuse); (2) onset of ataxia in association with stroke, encephalitis, sepsis, hyperthermia, or heat stroke; (3) chronic diarrhea; (4) unexplained visual loss; (5) malignancies; (6) rapid progression (defined as the development of severe ataxia in less than 12 weeks); or (7) insulin-dependent diabetes mellitus. In addition, the clinical criteria for multiple system atrophy (MSA) [11] were assessed to distinguish SAOA from MSA-C. All participants fulfilling the criteria for probable MSA-C (namely autonomic failure involving urinary incontinence or orthostatic dysregulation) were classified as MSA-C and not included in the SAOA cohort.

The clinical assessment of the SAOA patients included the Scale for the Assessment and Rating of Ataxia (SARA) [12]. The SARA score is comprised of eight items, including tests of gait, stance, sitting, speech, and ataxia of the upper and lower limb. The score ranges from 0 to 40, where a higher score indicates a greater impairment and has been used as a primary measure of disease severity. All participants were genetically screened to exclude the most common spinocerebellar ataxias (SCA1, 2, 3, and 6). If cerebellar atrophy was absent, a genetic screening for Friedreich's Ataxia was performed. If the clinical phenotype included prominent tremor or cognitive impairment and MRI showed impairment and signal abnormalities in the middle cerebellar peduncles, the patients were tested for FMR1 permutation to exclude FXTAS (Fragile X-associated tremor/ataxia syndrome). In the supplement, a detailed description of clinical workup is given (Table S1). Initially, 46 SAOA patients were included in this study, but for technical reasons, 9 participants had to be excluded (4 × incomplete MRI data sets, 2 × incomplete clinical characterizations, 3 × insufficient data quality, i.e., motion artifacts). In addition, 51 healthy controls (HCs) in a comparable age range were taken from the healthy population recruited within other multicenter studies of the German Center of Neurodegenerative Diseases (DZNE e.V.) that used the same imaging protocol. In detail, healthy controls participated in the DELCODE project [13]. From this cohort, 49 HCs were finally included in the analysis. One HC had to be excluded due to incomplete MR data, and one data set had to be dismissed due to severe head motion. Detailed demographic and clinical characteristics of all participants are reported in Table 1.

### MRI Acquisition

MRI was acquired at two sites (Magdeburg and Bonn) using a 3 Tesla Tim Trio MR systems (Siemens Medical Systems, Erlangen, Germany). Both centers were equipped with the same gradient system, MR head coils, and used the same software release and MR protocols.

For the structural MRI data, isotropic high-resolution T1-weighted images were acquired using a magnetization-

**Table 1** Demographics and clinical characteristics of all participants

	HCs ( <i>n</i> = 49)	SAOA ( <i>n</i> = 37)	<i>p</i> value*
Age (years)	65.08 ± 6.85 (48–78)	62.38 ± 9.53 (41–78)	0.39
Gender (male/female)	20/29	22/15	0.27
Site (BN/MD)	23/26	9/28	0.09
Age of onset (years)	/	55.62 ± 9.08 (40–74)	/
Duration (years)	/	7.11 ± 5.81 (1–23)	/
SARA score	/	11.59 ± 6.16 (2–31)	/

Data are presented as mean ± SD (min-max). *SAOA*, sporadic ataxia with adult onset; *HCs*, healthy controls; *BN*, Bonn; *MD*, Magdeburg; *SARA*, scale for the assessment and rating of ataxia

\*Bonferroni corrected

prepared rapid gradient-echo sequence (MPRAGE). The scan parameters were as follows: TR = 2500 msec, TE = 4.37 msec, TI = 1100 msec, FA = 7°, GRAPPA acceleration  $R = 2$ , FOV = 256 mm, acquisition matrix = 256 × 256, 176 sagittal slices, slice thickness = 1 mm.

The MRI protocol for the resting-state fMRI images consisted of a standard T2\*-weighted gradient-echo EPI sequence with the following scan parameters: TR = 2580 msec, TE = 30 msec, FA = 80°, GRAPPA acceleration  $R = 2$ , FOV = 224 mm, acquisition matrix = 64 × 64, 47 slices and slice thickness = 3.5 mm. A total of 180 volumes were acquired within one run. Subjects were instructed to lie still with their eyes closed in the scanner and not fall asleep during resting-state scans.

## Data Preprocessing

### Voxel-Based Morphometry Analysis of the Cerebellum

The structural MRI data were preprocessed and analyzed using the SUIT toolbox [5]. The images were cropped in order to isolate the cerebellum and were then segmented into its gray (GM), white matter (WM), and cerebrospinal fluid (CSF) compartments in individual space. For each subject, a cerebellum mask was automatically generated. Any misclassifications of the cerebellar boundaries were manually corrected using FSLView [14]. The normalization of the isolated cerebellum into a cerebellar template provided by SUIT was achieved using the “Diffeomorphic Anatomical Registration using Exponentiated Lie Algebra” (DARTEL) algorithm [15]. In order to preserve the local tissue volume during this procedure, the individual GM and WM maps were multiplied by the determinant of the Jacobian matrix of the deformation field (modulation). The resulting “modulated” normalized GM maps were finally smoothed with a 4 mm Gaussian smoothing kernel (FWHM = 4 mm).

### rs-fMRI Data Preprocessing

Data preprocessing and analyses were performed using SPM12.<sup>1</sup> It included slice timing, realignment, and normalization. From the motion correction parameters (3 translations, 3 rotations), we calculated additional parameter like the maximum displacement, its root mean square, and the mean frame-wise displacement to better characterize the motion-induced noise in the rs-fMRI time series. In total, we calculated 24-parameter motion profiles on an individual basis (no difference between the SAOA and HC groups;  $p > 0.05$ ). The realigned functional images were transformed into SUIT space using a non-linear deformation algorithm after co-registration the functional scans to the structural volume in native space. The functional scans were resliced to a voxel size of 2 × 2 × 2 mm<sup>3</sup>. In the temporal domain, we followed the standard procedures for preprocessing resting-state data, removing any linear trend and applying a band-pass filter (0.01–0.08 Hz). Previous studies have suggested signal changes in the white matter (WM) and cerebrospinal fluid (CSF) primarily reflect non-neural fluctuations like physiological artifacts (e.g., breathing, heart frequency) [16, 17]. In order to remove physiological noise components, the mean bold signal across the WM and CSF partition as well as the individual 24-parameter motion profiles was regressed out from each voxel’s time series [18].

### ALFF and DC Calculation

The amplitude of low-frequency fluctuation (ALFF) and degree centrality (DC) was calculated using the freely available, MATLAB-based GREYNA\_2.0 toolbox [19].

ALFF calculations were performed as previously described [6]. Briefly, the time series were first transformed to the frequency domain using a fast Fourier transform. The square root of the power spectrum, which was obtained from a predefined frequency interval (0.01–0.08) at each voxel, was calculated

<sup>1</sup> <https://www.fil.ion.ucl.ac.uk/spm/software/spm12>

and averaged. The averaged square root is defined as ALFF. To reduce the global effects of variability across the participants, the ALFF of each voxel was divided by the global mean ALFF for each participant. The resulting maps were spatially smoothed (FWHM = 4 mm) before entered into the statistical analysis as described below.

For the DC calculations, we followed the procedure suggested by Wang and colleagues [19]. In a first step, we defined a cerebellum mask of the GM including only voxels with non-zero variance over time for all participants and voxel that has at least a probability being a GM voxel of 20%. Within this, the resulting mask, a Pearson correlation between every voxel, was calculated. Voxels were considered to be connected with each other when the pairwise correlation coefficient was larger than 0.29 [9]. DC was calculated as the sum of weights (correlations) over connecting edges [8, 9]. The resulting individual DC maps were converted into Fisher  $z$  value maps and smoothed spatially with a Gaussian kernel (FWHM = 4 mm).

## Statistical Analysis

All statistical analysis was performed using MATLAB (R2013, The MathWorks, Inc. Natick, Massachusetts, USA). The demographic variables were analyzed using two-sample  $t$  test (age) and chi-square test (gender and site). Bonferroni corrected  $p$  values of less than 0.05 were considered statistically significant.

## Structural MRI Analysis

To examine structural differences between both groups on a voxel by voxel level of the GM partition, we set up a linear model including age, gender, imaging site, and total intracranial volume (ICV) as covariates of no interest, and applied a two-sample  $t$  test. The multiple comparison correction was performed using family-wise error (FWE) corrected  $p < 0.01$  (height-threshold FWE-corrected  $p < 0.01$ , extent-threshold cluster size  $> 337$ ).

To assess the relationship between altered GM in SAOA patients with clinical assessments, we averaged the GM voxel values across the different regions showing a significant volume reduction and performed separate partial correlations between the regional mean GM volume and the SARA total sum score, disease duration, and disease onset, parceling out the effect of age, gender, imaging site, and ICV. Bonferroni correction was applied using family-wise error (FWE) corrected  $p < 0.01$  (height-threshold FWE-corrected  $p < 0.01$ , extent-threshold cluster size  $> 314$ ).

## rs-fMRI Analysis

In order to investigate the functional characteristics in altered GM regions, we first compared if there is altered ALFF in regions showing altered GM volume in SAOA patients, controlling for age, gender, and imaging site. In a second step, the mean ALFF of the altered GM regions was compared with the overall mean ALFF of the unaffected cerebellar regions. This was achieved using a permutation test. This approach was chosen, because the affected regions cover a much smaller volume ( $n_1 = 9945$  voxels) than the unaffected part of the cerebellum ( $n_2 = 168,993$  voxels), not allowing for a direct comparison of the mean values via a simple  $t$  test. The permutation testing was performed by randomly extraction of  $n_1$  voxels from the unaffected parts ( $n_2$  voxels) and calculating the mean ALFF for this selection. This procedure was repeated 10,000 times to generate an empirical null distribution of “simulated” mean ALFF values. Using this distribution, one can test if the mean ALFF of the affected regions deviates significantly from the derived null distribution. The same procedures were repeated for the DC maps for both groups. All the ALFF and DC maps were resliced to 1-mm resolution in order to fit the spatial resolution of the structural MRIs.

## Results

### Demographics and Clinical Characteristics

Table 1 summarizes the demographic information of both groups, and the clinical characteristics for the SAOA patients finally included in the image analysis. The HC and SAOA patients showed no significant group difference in age ( $t = 1.53$ ,  $p = 0.39$ ) and sex ( $\chi^2 = 2.93$ ,  $p = 0.27$ ) but an unequal site distribution with less SAOA patients included in Bonn ( $\chi^2 = 4.63$ ,  $p = 0.09$ ).

### Voxel-Based Morphometry of Cerebellum

SAOA patients showed a significant mostly bilateral GM reduction in lobules I–IV, V, VI, IX, X, and vermis portion related to lobule VIII a/b in comparison with the HC group. The results are visualized on the surface flatmap template provided by SUIT (Fig. 1). All cerebellar regions showing a significant GM reduction are listed in Table 2.

### Correlation Between Altered GM Volume and Clinical Parameters

A negative correlation was found between GM volume of lobule X and SARA sum score ( $r = -0.60$ ,  $p < 0.001$ ). The GM volumes of lobules I–IV–V–VI significantly correlated negatively with disease duration ( $r_{I-IV} = -0.55$ ,  $r_V = -0.58$ ,



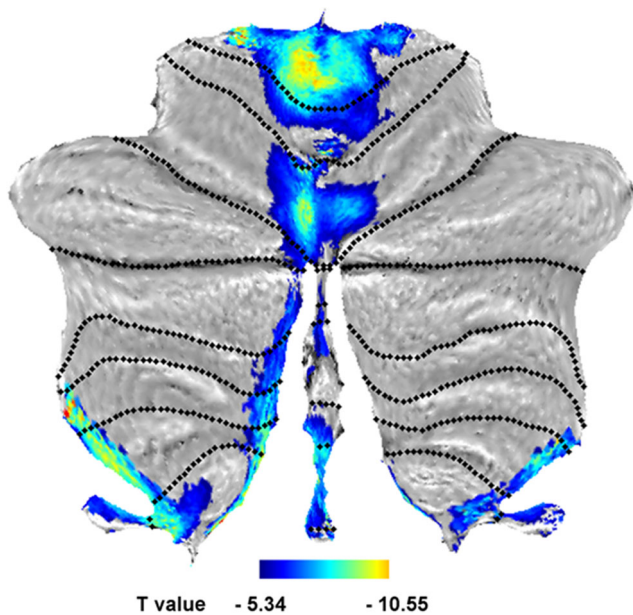


**Fig. 1** Between groups voxel-based comparison of cerebellar GM volume. Regions of reduced GM volume involved bilateral lobules I–IV, V, VI, IX, X, and vermis VIII a/b in SAOA patients compared with HCs are reported and mapped on the SUIT surface. The multiple comparison correction was performed using family-wise error (FWE) corrected  $p < 0.01$  (height-threshold FWE-corrected  $p < 0.01$ , extent-threshold cluster size  $> 337$ )

$r_{VI} = -0.57$ , all  $p < 0.001$ ), and positively correlated with age of disease onset ( $r_{I-IV} = 0.54$ ,  $r_V = 0.57$ ,  $r_{VI} = 0.56$ , all  $p < 0.001$ ) (Fig. 2).

### Characteristics of ALFF in Regions with Altered GM Volume

The SAOA patients showed a trend towards an increased spontaneous neuronal activity of the affected regions ( $ALFF_{HC} < ALFF_{SAOA}$ ,  $p = 0.059$ ). The permutation test also revealed that those clusters exhibiting gray matter atrophy were characterized by high ALFF values. This was the case in both groups, the SAOA patients and the HCs. None of simulated mean ALFF (HC,  $25.89 \pm 0.08$ ; SAOA,  $27.91 \pm 0.08$ ) was larger than our observed real mean ALFF (HC,

$32.67 \pm 12.07$ ; SAOA,  $35.75 \pm 14.93$ ,  $p < 0.001$ ). The results are summarized in Fig. 3.

### Characteristics of DC in Regions with Altered GM Volume

In the GM atrophy regions, no DC group differences were observed. However, the consecutive permutation test revealed that the atrophic regions were poorly connected regions in the cerebellar network compared with the unaffected parts of the cerebellum. This holds true for both groups. All randomly generated mean DC was significantly larger in both groups compared with the overall averaged DC values (permutation,  $DC_{HC} = 414.70 \pm 1.36$ ; atrophy region,  $DC_{HC} = 339.43 \pm 211.96$ ,  $p < 0.001$ ; permutation,  $DC_{SAOA} = 494.09 \pm 1.49$ ; atrophy region,  $DC_{SAOA} = 426.09 \pm 397.62$ ,  $p < 0.001$ ). The results are outlined in Fig. 4.

## Discussion

In the current study, we investigated the structural abnormalities in the cerebellum in SAOA and further explored the functional features associated with these structures. In SAOA patients, when compared with HC, significant GM atrophy was observed in bilateral cerebellar lobules I–IV, V, VI, IX, X, and vermis portion related to VIII a/b. In general, these findings are in line with the study from Abele and colleagues but reveal a more detailed picture [1] by showing that GM alterations are highly correlated with the clinical features. Even though these regions differ between groups with respect to the local gray matter volume, no alteration in ALFF or in DC was found in SAOA. However, when exploring the functional features of the atrophic regions, we found higher ALFF and lower DC values compared with unaffected cerebellar regions. This finding was not restricted to the patient group but was also observed for the HCs.

Using the cerebellar atlas provided by SUIT, its advanced preprocessing pipeline using DARTEL, and the flatmapping technique allowing for small smoothing kernels, enabled us to

**Table 2** Regions showing significant gray matter atrophy in SAOA patients

Cerebellar region	Peak coordinate (mm)			T value	p value	Cluster size (mm <sup>3</sup> )
	x	y	z			
I–IV	–2	–55	–21	10.554	<0.001	4259
V	–3	–67	–16	7.206	<0.001	978
VI	–3	–76	–20	7.431	<0.001	1888
IX	–5	–58	–33	9.111	<0.001	975
X	–26	–39	–41	7.757	<0.001	538
Vermis VIII a/b	–6	–59	–34	8.553	<0.001	409

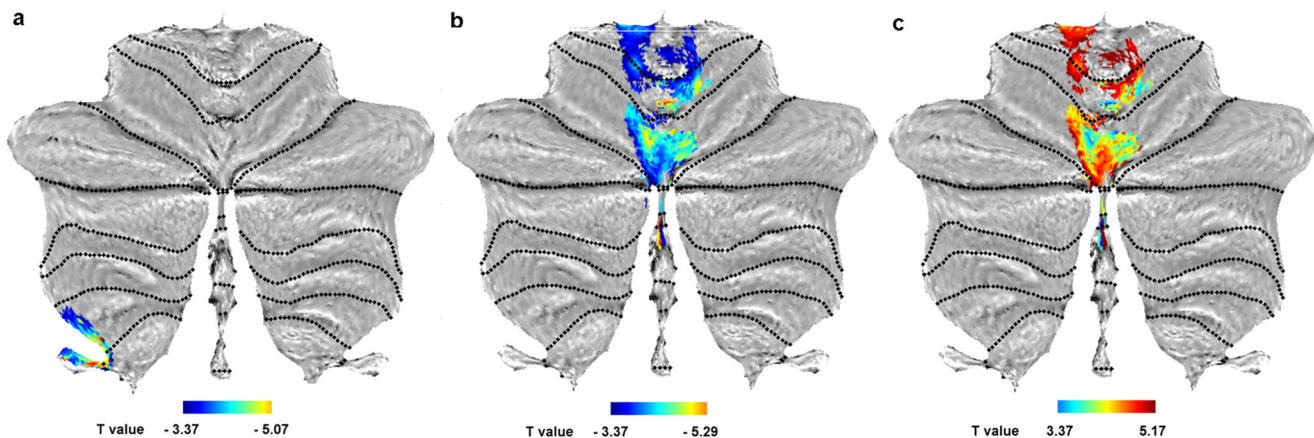


**Fig. 2** Correlation between altered GM volume and clinical assessment. Flatmap plots demonstrating the association between **a** GM volumes of lobule X and SARA, **b** GM volumes of lobules I–IV–V–VI and duration, **c** GM volumes of lobules I–IV–V–VI and age of onset. Correction for

multiple comparisons was performed using FWE-corrected  $p < 0.01$  (height-threshold FWE-corrected  $p < 0.01$ , extent-threshold cluster size  $> 314$ )

map morphological changes in SAOA at the cerebellar level with a higher effective spatial resolution as compared with the Abele and colleagues [1]. The spatial distribution of the atrophy found in the SAOA group corresponded to the clinical presentation of SAOA. We found a cluster with significant GM atrophy including anterior cerebellum (bilateral I–IV, V). The anterior cerebellum is highly involved in motor and sensorimotor processing, e.g., motor dexterity, coordination, and complex movement integration [20] suggesting that the

gray matter loss in these regions contributes to ataxia in SAOA. Furthermore, lobules V and VI have strong primary somatosensory representation [21–23]. Lobule V contains representation of upper-limb movements, while lobule VI is reported to be involved in lower-limb movements [22, 24]. Atrophy in lobules V–VI is in line with prominent limb coordination deficits typical for SAOA [1, 25]. It is also noteworthy that the alterations of GM volume in lobules I–VI correlated with both disease duration and age of onset. Even though

**Fig. 3** Characteristics of ALFF in regions with altered GM volume. Flatmaps show the ALFF distribution within the cerebellum for both groups (**a** HC group; **b** SAOA group). The regions showing significant atrophy are outlined with black lines. **c** Histograms plot distribution of generated mean ALFF in two groups. Green dot represents real ALFF of atrophy clusters in the HC group while red dot represents the SAOA group

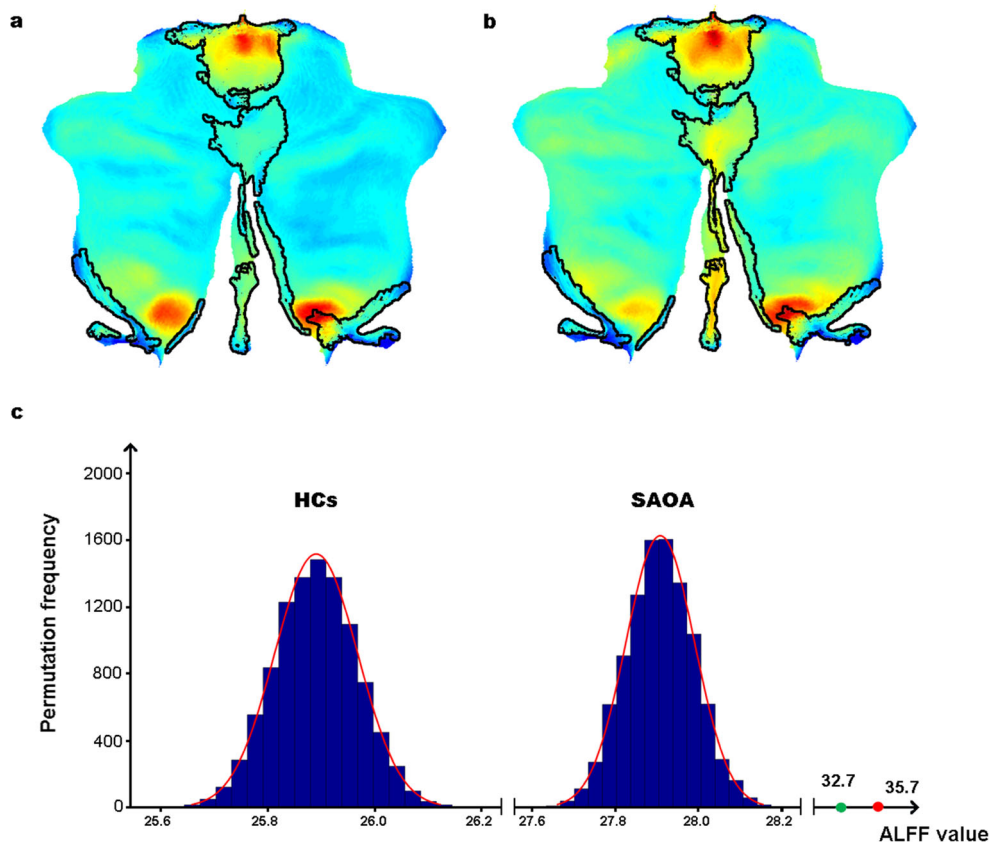
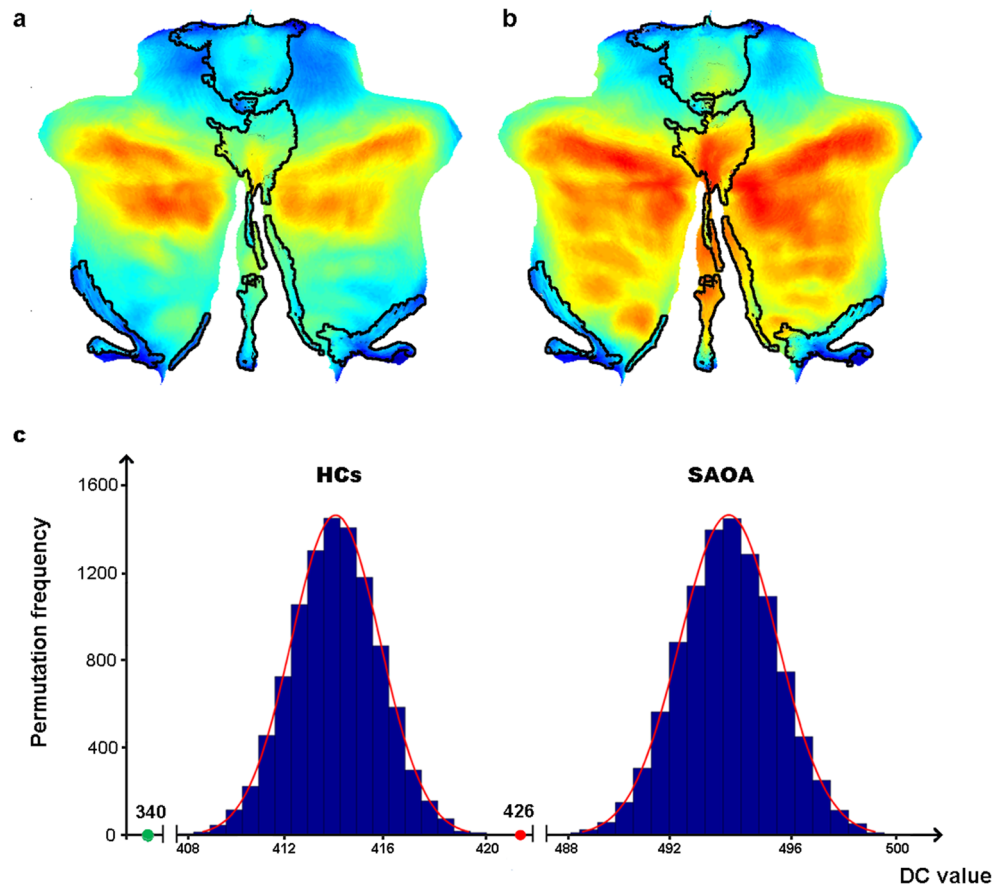


**Fig. 4** Characteristics of DC in regions with altered GM volume. Flatmaps show the DC distribution within the cerebellum for both groups (**a** HC group; **b** SAOA group). Regions showing significant atrophy are outlined with black lines. **c** Histograms plot distribution of generated mean DC in two groups. Green dot represents real DC of atrophy clusters in the HC group while red dot represents the SAOA group



our results are based on cross-sectional data, they are in line with the clinically progressive disease course of SAOA. On the other hand, the GM volume reduction correlated with age of onset, indicating that patients with an early age of onset show more severe GM loss. One could thus hypothesize that earlier age of onset is related to a more severe course of the disease. However, as we detected a high association ( $r = -0.99$ ,  $p < 0.001$ ) in duration and age of onset, at this point, we cannot finally judge which of those parameters is the driving force.

Our VBM analysis also demonstrated that the cerebellum exhibits clear posterior vermis atrophy in SAOA patients. This is also in line with previous imaging findings by Abele et al. [1] and Baloh et al. [26] and may reflect the fact that on a cell level mainly the Purkinje neurons of the cerebellar vermis are affected in SAOA [27]. Previous studies have reported significant implications for the involvement of the posterior vermis in movement control as well as its contribution to movement disorders [28, 29]. The posterior vermis plays an important role in locomotion [30], especially the vermis portion close to lobule VIII [31], probably because this region receives dense input from other parts of the brain. Projections from the cerebral cortex to vermis VIII originates from arm, leg, and proximal body representations that are located within multiple cortical areas. Projections from the motor cortex to

vermis VIII are likely to send signals related to force, speed, motor direction, and movement execution [32]. If our speculation regarding the functional role of this input to vermis VIII is correct, the atrophy observed here may represent the morphological basis of SAOA-related movement disorder symptomatology.

In addition, decreased GM volume in bilateral cerebellar lobules IX–X might explain some clinical symptoms in SAOA. The impairments of lobules IX and X are frequently reported as being associated with abnormal eye movements [33, 34]. Previous lesions studies in lobules IX–X showed lobule IX lesions to cause nystagmus and impaired vestibular-ocular reflex suppression, while lobule X lesions typically result in downbeat fixation nystagmus [32]. As the hemispheric lobule X representing the flocculonodular part of the cerebellum is associated with oculomotor functions, the involvement of the neighboring vermal parts seems to be straightforward [35]. In addition, lobules IX and X have extensive connections with the vestibular nuclei [36]. As a consequence, atrophy of lobules IX–X might lead to dysfunction of visual [37] and vestibular projections [38]. When correlating GM volume with SARA sum score as a proxy for disease severity, we identified significant voxels in cerebellar hemispheric lobule X. Therefore, this might represent the link between macroscopic pathology and clinical phenotype.



Considering that lobules IX–X are also reported to be involved in a cognitive performance like episodic memory, self-reflection, facial emotions, and associated functions [39, 40]; this observation of GM loss might also explain some of the cognitive deficits observed in SAOA [27, 41].

As discussed above, the SAOA patients showed cerebellar atrophy in regions consistently involved in motor and somatosensory processing [2]. Interestingly, none of these regions differs in local ALFF or DC between groups. Even though the local GM volume is reduced in these regions in SAOA, neither the local spontaneous activity accessed by ALFF nor the intra-cerebral functional connectivity characterized by DC seems to be affected. This unexpected finding may indicate a relatively normal neural activity and network integration. In fact, we found a trend towards even increased neural activity in those regions and one may speculate that this finding represents a functional compensational mechanism. Comparing the ALFF and DC of the affected regions with the rest of the cerebellum, our data revealed that the affected regions had higher local spontaneous neural activity and lower functional intra-cerebellar connectivity compared with the rest of the cerebellum. Because this finding is observed in both populations, one can argue that this observation is not caused by SAOA-related pathological processes. It suggests that those regions with high ALFF and low DC might be more vulnerable to SAOA pathology.

A relevant limitation of this study is the lack of longitudinal data. In addition, the presumed heterogeneity of SAOA may limit the statistical power and reproducibility of our results. A principal problem in the clinical diagnosis of SAOA is the delineation from MSA-C which fully relies on clinical criteria [2]. Considering there is a situation that some SAOA patients will convert to MSA-C in the disease progression, we extracted a SAOA subgroup (Supplementary Table S1) which only included SAOA patients with symptom duration larger than 10 years [2]. Even though the number of participants is largely reduced, the subgroup analysis replicates our reported finding (Supplementary Table S2 and Supplementary fig. S1). Therefore, it is not very likely that our results are biased by those patients that might convert in the future.

## Conclusion

Our data revealed a volume reduction in SAOA in regions that are known to be involved in motor and somatosensory processing. This is in line with the clinical appearance of SAOA. Our data suggest that the atrophy occurs in those cerebellar regions which are characterized by high ALFF and poor DC. Further studies have to show if these findings are specific for SAOA and if they can be used to predict disease progression.

## Compliance with Ethical Standards

The study was approved by the local ethics committees in Bonn and Magdeburg. All subjects provided written informed consent before participation.

**Conflict of Interest** The authors declare that they have no conflict of interest.

## References

1. Abele M, Minnerop M, Urbach H, Specht K, Klockgether T. Sporadic adult onset ataxia of unknown etiology: a clinical, electrophysiological and imaging study. *J Neurol*. 2007;254(10):1384–9.
2. Giordano I, Harmuth F, Jacobi H, Paap B, Vielhaber S, Machts J, et al. Clinical and genetic characteristics of sporadic adult-onset degenerative ataxia. *Neurology*. 2017;89(10):1043–9.
3. Klockgether T. Sporadic ataxia with adult onset: classification and diagnostic criteria. *Lancet Neurol*. 2010;9(1):94–104.
4. Ota S, Tsuchiya K, Anno M, Niizato K, Akiyama H. Distribution of cerebello-olivary degeneration in idiopathic late cortical cerebellar atrophy: clinicopathological study of four autopsy cases. *Neuropathology*. 2008;28(1):43–50.
5. Diedrichsen J. A spatially unbiased atlas template of the human cerebellum. *NeuroImage*. 2006;33(1):127–38.
6. Zang YF, He Y, Zhu CZ, Cao QJ, Sui MQ, Liang M, et al. Altered baseline brain activity in children with ADHD revealed by resting-state functional MRI. *Brain and Development*. 2007;29(2):83–91.
7. Zuo XN, Di Martino A, Kelly C, Shehzad ZE, Gee DG, Klein DF, et al. The oscillating brain: complex and reliable. *NeuroImage*. 2010;49(2):1432–45.
8. Buckner RL, Sepulcre J, Talukdar T, Krienen FM, Liu H, Hedden T, et al. Cortical hubs revealed by intrinsic functional connectivity: mapping, assessment of stability, and relation to Alzheimer's disease. *J Neurosci*. 2009;29(6):1860–73.
9. Zuo XN, Ehmke R, Mennes M, Imperati D, Castellanos FX, Sporns O, et al. Network centrality in the human functional connectome. *Cereb Cortex*. 2012;22(8):1862–75.
10. Premi E, Cauda F, Costa T, Diano M, Gazzina S, Gualeni V, et al. Looking for neuroimaging markers in frontotemporal lobar degeneration clinical trials: a multi-voxel pattern analysis study in granulin disease. *J Alzheimers Dis*. 2016;51(1):249–62.
11. Gilman S, Wenning GK, Low PA, Brooks DJ, Mathias CJ, Trojanowski JQ, et al. Second consensus statement on the diagnosis of multiple system atrophy. *Neurology*. 2008;71(9):670–6.
12. Schmitz-Hubsch T, du Montcel ST, Baliko L, Berciano J, Boesch S, Depondt C, et al. Scale for the assessment and rating of ataxia: development of a new clinical scale. *Neurology*. 2006;66(11):1717–20.
13. Jessen F, Spottke A, Boecker H, Brosseron F, Buerger K, Catak C, et al. Design and first baseline data of the DZNE multicenter observational study on predementia Alzheimer's disease (DELCODE). *Alzheimers Res Ther*. 2018;10(1):15.
14. Smith SM, Jenkinson M, Woolrich MW, Beckmann CF, Behrens TE, Johansen-Berg H, et al. Advances in functional and structural MR image analysis and implementation as FSL. *NeuroImage*. 2004;23(Suppl 1):S208–19.
15. Ashburner J. A fast diffeomorphic image registration algorithm. *NeuroImage*. 2007;38(1):95–113.
16. Dagli MS, Ingeholm JE, Haxby JV. Localization of cardiac-induced signal change in fMRI. *NeuroImage*. 1999;9(4):407–15.



17. Windischberger C, Langenberger H, Sycha T, Tschernko EM, Fuchsjaeger-Mayerl G, Schmetterer L, et al. On the origin of respiratory artifacts in BOLD-EPI of the human brain. *Magn Reson Imaging*. 2002;20(8):575–82.
18. Friston KJ, Williams S, Howard R, Frackowiak RS, Turner R. Movement-related effects in fMRI time-series. *Magn Reson Med*. 1996;35(3):346–55.
19. Wang J, Wang X, Xia M, Liao X, Evans A, He Y. GREYNET: a graph theoretical network analysis toolbox for imaging connectomics. *Front Hum Neurosci*. 2015;9:386.
20. Samson M, Claassen DO. Neurodegeneration and the cerebellum. *Neurodegener Dis*. 2017;17(4–5):155–65.
21. Buckner RL, Krienen FM, Castellanos A, Diaz JC, Yeo BT. The organization of the human cerebellum estimated by intrinsic functional connectivity. *J Neurophysiol*. 2011;106(5):2322–45.
22. Grodd W, Hulsmann E, Lotze M, Wildgruber D, Erb M. Sensorimotor mapping of the human cerebellum: fMRI evidence of somatotopic organization. *Hum Brain Mapp*. 2001;13(2):55–73.
23. Reetz K, Dogan I, Rolfs A, Binkofski F, Schulz JB, Laird AR, et al. Investigating function and connectivity of morphometric findings—exemplified on cerebellar atrophy in spinocerebellar ataxia 17 (SCA17). *NeuroImage*. 2012;62(3):1354–66.
24. Mottolise C, Richard N, Harquel S, Szathmari A, Sirigu A, Desmurget M. Mapping motor representations in the human cerebellum. *Brain J Neurol*. 2013;136(Pt 1):330–42.
25. Klockgether T, Schroth G, Diener HC, Dichgans J. Idiopathic cerebellar ataxia of late onset: natural history and MRI morphology. *J Neurol Neurosurg Psychiatry*. 1990;53(4):297–305.
26. Baloh RW, Yee RD, Honrubia V. Late cortical cerebellar atrophy. Clinical and oculographic features. *Brain J Neurol*. 1986;109(Pt 1):159–80.
27. Klockgether T. Sporadic adult-onset ataxia. *Handb Clin Neurol*. 2018;155:217–25.
28. Gellersen HM, Guo CC, O’Callaghan C, Tan RH, Sami S, Hornberger M. Cerebellar atrophy in neurodegeneration—a meta-analysis. *J Neurol Neurosurg Psychiatry*. 2017;88(9):780–8.
29. Shin H, Lee DK, Lee JM, Huh YE, Youn J, Louis ED, et al. Atrophy of the cerebellar vermis in essential tremor: segmental volumetric MRI analysis. *Cerebellum*. 2016;15(2):174–81.
30. Morton SM, Bastian AJ. Cerebellar control of balance and locomotion. *Neuroscientist*. 2004;10(3):247–59.
31. Schmitt JE, Eliez S, Warsofsky IS, Bellugi U, Reiss AL. Enlarged cerebellar vermis in William’s syndrome. *J Psychiatr Res*. 2001;35(4):225–9.
32. Kheradmand A, Zee DS. Cerebellum and ocular motor control. *Front Neurol*. 2011;2:53.
33. Beh SC, Frohman TC, Frohman EM. Neuro-ophthalmic manifestations of cerebellar disease. *Neurol Clin*. 2014;32(4):1009–80.
34. Beh SC, Frohman TC, Frohman EM. Cerebellar control of eye movements. *J Neuroophthalmol*. 2017;37(1):87–98.
35. Rondi-Reig L, Paradis AL, Lefort JM, Babayan BM, Tobin C. How the cerebellum may monitor sensory information for spatial representation. *Front Syst Neurosci*. 2014;8:205.
36. Barmack NH. Central vestibular system: vestibular nuclei and posterior cerebellum. *Brain Res Bull*. 2003;60(5–6):511–41.
37. Glickstein M, Gerrits N, Kralj-Hans I, Mercier B, Stein J, Voogd J. Visual pontocerebellar projections in the macaque. *J Comp Neurol*. 1994;349(1):51–72.
38. Yakusheva TA, Blazquez PM, Chen A, Angelaki DE. Spatiotemporal properties of optic flow and vestibular tuning in the cerebellar nodulus and uvula. *J Neurosci*. 2013;33(38):15145–60.
39. Habas C, Kamdar N, Nguyen D, Prater K, Beckmann CF, Menon V, et al. Distinct cerebellar contributions to intrinsic connectivity networks. *J Neurosci*. 2009;29(26):8586–94.
40. Scharmuller W, Ille R, Schienle A. Cerebellar contribution to anger recognition deficits in Huntington’s disease. *Cerebellum*. 2013;12(6):819–25.
41. Berent S, Giordani B, Gilman S, Trask CL, Little RJ, Johanns JR, et al. Patterns of neuropsychological performance in multiple system atrophy compared to sporadic and hereditary olivopontocerebellar atrophy. *Brain Cogn*. 2002;50(2):194–206.

**Publisher’s Note** Springer Nature remains neutral with regard to jurisdictional claims in published maps and institutional affiliations.